International Journal of Technology

http://ijtech.eng.ui.ac.id

Research Article

Green Synthesis of TiO_2 Nanoparticles with *Melastoma malabathricum* Fruit Extract and Lime Juice: Toward Efficient Dye-Sensitized Solar Cell Photoanodes

Muhammad[1], Nofrijon Sofyan[1,2*], Akhmad Herman Yuwono[1,2], Donanta Dhaneswara[2], Mouna M'rad[3]

[1]Department of Metallurgical and Materials Engineering, Faculty of Engineering, Universitas Indonesia, Depok 16424 Indonesia

[2]Advanced Materials Research Center, Faculty of Engineering, Universitas Indonesia, Depok 16424 Indonesia

[3]Department Physique, Université Paris-Saclay, Bâtiment Bréguet, 91190, France

[*]Corresponding author: nofrijon.sofyan@ui.ac.id; Tel.: + 62-21-7863510; Fax.: +62-21-7872350

Abstract: This study investigates the eco-friendly synthesis of TiO_2 NPs using Melastoma malabathricum fruit extract and lime juice as natural reducing and capping agents. The extract was prepared by macerating the sample in ethanol. TiO_2 NPs were synthesized via the sol–gel method with five variations: one control sample using ethanol only and four samples incorporating plant extracts with varying lime juice concentrations. The results confirmed the formation of pure anatase-phase TiO_2 with crystallite sizes decreasing from 18.17 to 12.43 nm. Optical analysis revealed bandgap energies of 3.09-3.14 eV, suitable for dye-sensitized solar cell (DSSC) applications. The field-emission scanning electron microscopy (FESEM) images revealed more uniform, smaller particles in the capped samples, as supported by the particle-size distribution data. energy-dispersive X-ray spectroscopy (EDX) confirmed that the elemental composition is close to stoichiometric TiO_2. Electrochemical analysis indicated that the sample using Melastoma malabathricum fruit extract exhibited superior photovoltaic performance (power conversion efficiency (PCE) = 3.12%) owing to enhanced charge injection, despite a shorter electron lifetime (55 ms). Additionally, samples using Melastoma malabathricum fruit extract and lime juice exhibited improved charge retention (τ_e = 205-274 ms), despite their moderate efficiencies (2.26-2.49%). This study demonstrates the significant potential of tropical plant-mediated synthesis for developing sustainable, high-performance DSSC photoanodes, with performance governed by careful optimization of the composition of natural capping agents.

Keywords: Dye-sensitized solar cell; Lime juice; *Melastoma malabathricum*; Nanoparticles; Photoanode; Titanium dioxide

1. Introduction

The urgency of transitioning to sustainable energy systems has grown in recent years, driven by global energy insecurity exacerbated by post-pandemic disruptions, climate change, and geopolitical tensions (Hussain et al., 2023). In this context, solar energy is a promising alternative, particularly for tropical countries, such as Indonesia, which receive abundant sunlight year-round (Boediman et al., 2021). Despite this potential, the adoption of solar technologies remains limited, primarily due to the high cost and technical complexity of conventional photovoltaic systems (Siagian et al., 2024). Dye-sensitized solar cells (DSSCs) have attracted attention as a third-generation solar technology, offering several advantages, including cost-effectiveness, versatility, and ease of fabrication (Ibrahim et al., 2025). This device operates on light absorption by dye molecules, which excite electrons and inject them into a semiconducting photoanode to produce electrical energy (Sofyan et al., 2017). Recently, small-scale DSSC devices have been developed for real-world applications, including indoor sensors, Internet of Things devices, and

https://doi.org/10.14716/ijtech.v17i3.8319
Received July 2025; Revised January 2026; Accepted February 2026

building-integrated photovoltaics (Szindler et al., 2021; Devadiga et al., 2021). Their potential has also been highlighted in tropical regions such as Indonesia, where DSSC-based transparent photovoltaics and BIPV systems have been simulated and demonstrated significant energy savings of up to 59.3% in building applications, along with strong suitability for local climates (Hendinata et al., 2024; Rababah et al., 2021).

TiO_2 nanoparticles (TiO_2 NPs) are commonly used as a semiconductor layer in DSSCs owing to their high surface area, chemical stability, and strong photoelectronic properties (Drygala, 2021; Karim et al., 2019; Tyas et al., 2017). The choice and quality of the TiO_2 photoanode are critical to DSSCs' efficiency and overall performance (Muhammad et al., 2025). Among the various phases, anatase is the most suitable for DSSC applications due to its superior electron transport and low recombination rates (Roy et al., 2019; Yan et al., 2013). Its application enables high dye-loading capacity and efficient charge collection, which are essential for achieving favorable DSSC performance (Eddy et al., 2023). However, traditional methods for synthesizing TiO_2 NPs often involve hazardous chemicals, high energy consumption, and complex equipment, making them less environmentally friendly (Xu and Chen, 2020; Bhagoria et al., 2019; Yadav et al., 2015).

Green synthesis technologies have gained prominence over the past decade amid the rapid depletion of natural resources, offering a sustainable approach to producing nanostructured materials (Septiningrum et al., 2026). This approach avoids high-pressure reactors and high temperatures while minimizing polluting residues and yielding biodegradable products by employing natural agents such as plants, fruits, flowers, algae, or microbial extracts, with plant extracts proving especially viable (Rao et al., 2015). The presence of phytochemicals, such as flavonoids, phenolics, and organic acids, in these natural extracts contributes to particle formation, stabilization, and size control (Thiurunavukkarau et al., 2022). Several studies have demonstrated the successful use of various botanical sources for synthesizing TiO_2 NPs with improved morphological and optical properties suitable for DSSCs. Gambier leaf (Sofyan et al., 2025a), tropical almond (Sofyan et al., 2024), Carica papaya (Kaur et al., 2019), Aloe vera (Dülger et al., 2024), and Citrus sinensis (Singh et al., 2022) are some examples.

Melastoma malabathricum, a wild tropical plant with high flavonoid content, particularly in its fruit, is an underexplored botanical resource (Isnaini et al., 2019). These bioactive compounds exhibit strong reducing capacity and can stabilize nanostructures during synthesis (Saini and Kumar, 2023; Marslin et al., 2018; Liu et al., 2018). Additionally, lime juice, which contains citric and ascorbic acids, may provide additional benefits as a co-reducing and chelating agent, further enhancing nanoparticle formation and surface functionality (Bellè et al., 2023). The synergistic use of Melastoma malabathricum fruit extract and lime juice for the green synthesis of TiO_2 has not yet been thoroughly investigated, particularly regarding its impact on DSSC performance. Hence, there is a critical need to explore this approach further to produce TiO_2 nanoparticles with desirable physicochemical properties and to improve the energy conversion efficiency in DSSCs. In particular, understanding how bio-derived chelating agents influence the interfacial charge-transfer kinetics at the TiO_2–electrolyte interface is key to improving DSSC performance.

This study focuses on the green synthesis of TiO_2 nanoparticles using Melastoma malabathricum fruit extract as a natural reducing and capping agent under varying concentrations of natural lime juice extract as the chelating agent. Subsequently, the synthesized nanoparticles were used as photoanodes in a DSSC device to assess the effectiveness of tropical plant-based materials in solar energy applications.

2. Experimental Setup

2.1 Materials

Titanium tetraisopropoxide ($Ti[OCH(CH_3)_2]_4$, 97%) from Sigma-Aldrich (St. Louis, MO, USA) was used as the synthesis precursor. Other chemicals, including ethanol (99.9%), N-

methyl-2-pyrrolidone (NMP), and polyvinylidene fluoride (PVDF), were obtained from Merck (Darmstadt, Germany), and Platisol T/SP, Ruthenizer 535-bis TBA (N719), iodolyte HI-30, and Meltonix 1170-60 were obtained from Solaronix SA (Aubonne, Switzerland). Indium-doped tin oxide (ITO) (1.1 mm thick, sheet resistance 6 ohms/square) was used as the conducting glass for this experiment.

2.2 Lime Juice and Melastoma malabathricum Extract Preparations

Fresh Melastoma fruits were collected from a wild-growing population in an open field in Bogor, Indonesia, and dried for 6 h at 50°C using a dehydrator. A 10 g sample of dried fruit was ground and extracted with 50 ml of ethanol containing 0%, 20%, 40%, or 50% lime juice. Fresh limes were manually squeezed to obtain lime juice, which was subsequently filtered to remove pulp and insoluble solids. Clarified lime juice was added to the extraction solvent to adjust the pH and serve as a chelating agent (Sangeetha et al., 2024). The mixture was filtered to separate the insoluble residue from the solvent, yielding Melastoma fruit extracts. The extracts were then used to green-synthesize TiO_2 NPs.

2.3 Green Synthesis of TiO_2 Nanoparticles

The environmentally friendly synthesis of titanium oxide was carried out following the sol–gel method. Five beakers were prepared, each containing 5 mL of titanium tetraisopropoxide (TTIP). For the control sample (C1), 80% ethanol (6.25 mL) was added dropwise to the first beaker. For the remaining beakers, 6.25 mL of Melastoma malabathricum fruit extract prepared using different ethanol–lime juice solvent compositions, as described in Section 2.2, was added dropwise, and the samples were labeled M1, M2, M3, and M4, respectively (Table 1).

The mixture was stirred on a magnetic stirrer for 2 hours, then filtered to yield a wet gel. The wet gel was dried at 80 °C for 8 hours, then calcined at 450 °C for 2 hours and 30 minutes. The resulting TiO_2 nanopowders synthesized under different solvent conditions were collected and used in further characterization and application studies. To facilitate a clearer understanding of the overall workflow for the green synthesis of TiO_2 nanoparticles, from extract variation and sol–gel processing to structural confirmation, a flowchart is shown in Figure S1, Supplementary.

2.4 Fabrication of solar cells

Solar cell devices were fabricated by modifying the procedure in our previous work (Sofyan et al., 2024) with slight modifications. In this study, five sensitized devices were prepared using N719 dye. For each sample variation (C1, M1, M2, M3, and M4), pairs of ITO conductive glass substrates were ultrasonically cleaned in acetone, followed by ethanol at room temperature. One of the ITO glass substrates was designated as the counter electrode, and the other served as the photoanode.

Table 1 Summary of sample codes (C1, M1-M4) used in TiO_2 nanoparticle synthesis

Code	Solvent Composition	Maceration Parameter		pH (measured)
		Ethanol (% v/v)	Lime Juice (% v/v)	
C1	-	-	-	-
M1	Ethanol	100	0	5
M2		80	20	4
M3	Ethanol + lime juice	60	40	4
M4		50	50	3

Two diagonal holes approximately 1 mm in diameter were drilled into the ITO glass substrate to prepare the counter electrode. An area of 1 cm^2 was obtained by masking the undeposited area of the conductive ITO glass substrate with a thin plastic tape prior to slurry coating. Platinum paste was then applied to the exposed area using the doctor blade technique.

After the plastic tape was removed, the coated substrate was heated to 400 °C for 30 minutes, then cooled to room temperature.

The photoanode preparation began with the formulation of a binder solution by heating 1.00 mL of NMP at 60 °C for 30 minutes in an enclosed container. Subsequently, 50.00 mg of PVDF powder was gradually added under constant low stirring, followed by continued stirring at 1000 rpm for an additional 30 minutes. From this binder solution, 10.00 μL was transferred into separate containers corresponding to each sample variation. A total of 90 mg of TiO_2 powder was deposited onto the conductive side of the ITO substrate using the doctor blade method over the same active area as the counter electrode. The coated photoanodes were dried at 65 °C for 2 h and then cooled to room temperature. A 0.8 mM N719 solution was prepared for the sensitizer by dissolving 50 mg of the powder in 50 mL of ethanol (Yum et al., 2011). The dried photoanodes were immersed in the dye solution for 12 h and then air-dried.

To prevent short circuits, the device was assembled by joining the photoanode and counter electrode using Meltonix 1170-60 as a spacer and sealant. The assembled cells were heated to 90 °C to ensure proper sealing and then cooled to room temperature. Finally, the iodolyte was carefully injected through one of the predrilled holes on the counter-electrode side until the entire volume was filled. Once completed, the holes were sealed, and the device was ready for examination of its photovoltaic performance.

2.5 Characterization

All characterization measurements were performed at room temperature under ambient laboratory conditions, without pressure or humidity control. Fourier transform infrared spectroscopy (FTIR) was conducted using a PerkinElmer ATR Spectrum One spectrometer (Waltham, MA, USA). Ultraviolet–visible diffuse reflectance spectroscopy (UV–Vis DRS) measurements were performed using a Shimadzu UV-2450 spectrophotometer (Kyoto, Japan). X-ray diffraction (XRD) analysis was performed on a Malvern Panalytical Empyrean diffractometer (Malvern, UK) to retrieve the crystallographic information from the samples. Raman spectroscopy measurements were conducted using a HORIBA iHR320 Raman spectrometer (Kyoto, Japan). Surface morphology and elemental composition were examined using a field-emission scanning electron microscope equipped with energy-dispersive X-ray spectroscopy (FE-SEM/EDX, FEI Inspect F50, Hillsboro, OR, USA). Electrochemical properties were evaluated using a Metrohm Autolab potentiostat (Utrecht, The Netherlands) under room-light conditions. Photovoltaic performance was measured using a Keithley 2450 source meter (Cleveland, OH, USA) coupled with an ABET Sunlite™ solar simulator (Milford, CT, USA) under standard illumination of 1000 W m^{-2} (AM 1.5G). All experimental procedures were performed at the Faculty of Engineering, Universitas Indonesia, except for Raman spectroscopy, which was conducted at the Integrated Laboratory Research Center (ILRC), Universitas Indonesia.

3. Results and Discussion

To provide a better understanding of the green synthesis route and its role in forming TiO_2 nanoparticles, a schematic illustration of the proposed green synthesis formation mechanism is proposed, which may involve several reaction steps as provided in Equations (1) – (3) (Polte, 2015).

1. Hydrolysis of titanium tetraisopropoxide

$$Ti(OCH(CH_3)_2)_4 + 4H_2O \rightarrow Ti(OH)_4 + 4(CH_2)_2CHOH \quad (1)$$

2. Condensation of amorphous hydrous titanium dioxide

$$Ti(OH)_4 \rightarrow TiO_2\_xH_2O + (2-x)H_2O \quad (2)$$

3. Nucleation and growth of the crystalline TiO_2 NPs during the calcination process

$$TiO_2{\_}xH_2O \rightarrow TiO_2 \quad (3)$$

At this stage, phytochemical compounds in the extract, such as flavonoids, are adsorbed onto the TiO_2 surface and act as capping agents, controlling and stabilizing growth. Furthermore, the obtained TiO_2 was deposited on the conductive glass surface to serve as the DSSC photoanode. The illustration of the TiO_2 formation process in this study is illustrated in Figure 1.

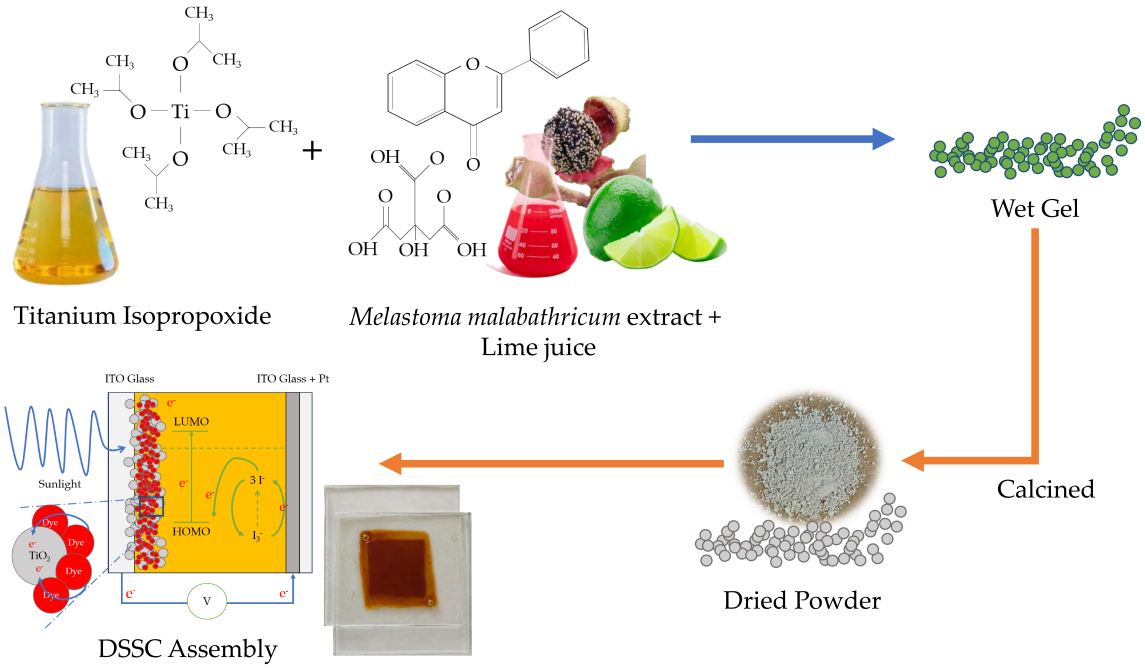

Figure 1 Formation mechanism illustration of TiO_2 NPs green synthesized in the presence of *Melastoma malabathricum* extract and lime juice

3.1 Identification of Functional Groups

FTIR characterization enables the identification of additional functional groups that may remain after TiO_2 synthesis. The observation was conducted over the range of 400–4000 cm^{-1}, as shown in Figure 2. Several distinct absorption bands were detected, which were attributable to functional groups arising from both the synthesis process and residual organic compounds. Table 2 summarizes the observed FTIR peaks, their assignments, and possible origins. The distinct peaks observed at 3354 cm^{-1} correspond to an O-H vibrational mode, likely arising from residual ethanol solvent and adsorbed moisture. Vibration at 2340 cm^{-1} (C-O bond), indicating the presence of organic residues from the green synthesis process. The absorption at 1682 cm^{-1} is assigned to the bending mode of the H–O–H bond in adsorbed water molecules. The prominent peak at wavenumber 1230 cm^{-1} and the broad band between 400 and 1050 cm^{-1} correspond to O–Ti–O and Ti–O–Ti lattice vibrations, respectively, confirming the formation of the TiO_2 crystalline structure (Singh et al., 2024).

3.2 Optical Properties

Bandgap energy is the energy that separates the valence band and the conduction band in a material. This property is crucial because it also indicates the material's ability to absorb photons at a specific wavelength (Zanatta, 2019). In this study, UV-Vis DRS was used to assess the optical properties of TiO_2 nanoparticles (NPs). To estimate the optical bandgap, the diffuse

reflectance data were calculated using the Kubelka-Munk relation given in Equation (4) (Makuła et al., 2018).

Table 2 Identification of functional groups from infrared spectra of as-synthesized TiO_2 NPs

Wavenumber (cm^{-1})	Functional Group	Assignment/Origin
3354	O–H stretch	Hydroxyl/volatile alcohol (from ethanol solvent, adsorbed water)
2340	C–O stretch	Organic residue possibly from green synthesis (phytochemicals, CO_2 adsorption)
1682	H–O–H bend	Absorbed water/ambient moisture
1230	O–Ti–O vibration	TiO_2 lattice
400–1050	Ti–O–Ti stretch	TiO_2 crystal structure

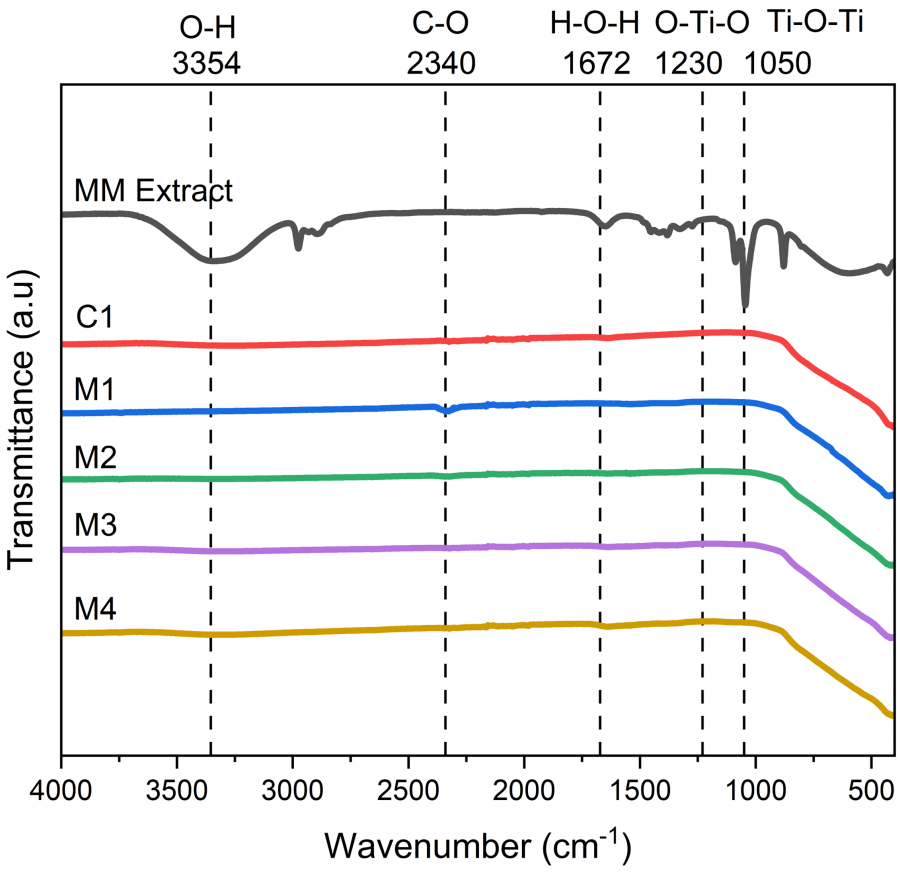

Figure 2 Infrared spectra of TiO_2 NPs synthesized using ethanol only (C1) and using *Melastoma malabathricum* extract with lime juice variations (M1, M2, M3, and M4)

$$(F(R_\infty) \cdot h\nu)^{1/\gamma} = B(h\nu - E_g) \tag{4}$$

where $F(R_\infty)$ denotes the Kubelka-Munk function, h denotes the Planck constant, v is the photon frequency, E_g represents the bandgap energy, B is constant, and γ is a factor that depends on the type of electronic transition, taking a value of ½ for direct transitions and 2 for indirect bandgap transitions. In this study, the bandgap energy was determined from the Tauc plot of $(F(R_\infty).hv)^{1/2}$ versus hv assumed an indirect allowed transition bandgap energy transition (Nagaraj et al., 2019). As shown in Figure 3, the corresponding Tauc's plot revealed the bandgaps for samples C1, M1, M2, M3, and M4 as 3.14, 3.12, 3.09, 3.09, and 3.10 eV, respectively.

The slight bandgap narrowing might be attributed to the incorporation or surface adsorption of organic species from the extract, which could introduce localized states within the bandgap (Sofyan et al., 2025a). Similar bandgap-narrowing mechanisms have been reported in doped TiO_2 nanoparticles, in which co-doping enhances visible-light absorption (Na-Phattalung et al., 2022). This bandgap narrowing is favorable for DSSC applications because it improves visible-light harvesting and facilitates more efficient electron injection and charge transport, thereby enhancing the overall PV performance (Villanueva-Cab et al., 2018).

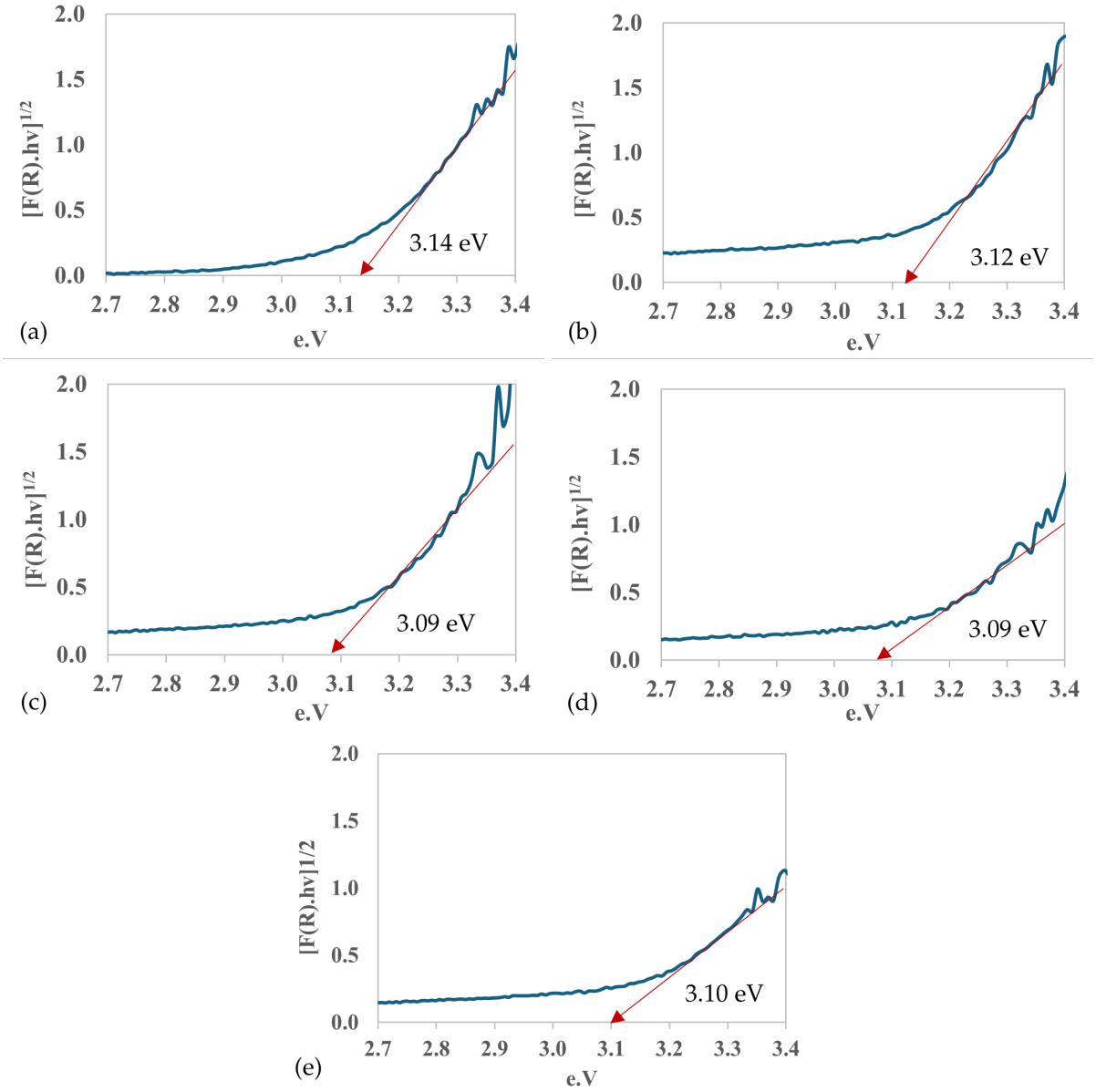

Figure 3 Tauc plots (F(R) $hv)^{1/2}$ versus photon energy (hv) of TiO_2 nanoparticles synthesized via sol–gel method using ethanol only (a) C1, and *Melastoma malabathricum* extract with lime juice variations (b) M1, (c) M2, (d) M3, and (e) M4. The red arrow points to the bandgap energy

3.3 Surface morphology and composition

In this study, the surface morphology of green-synthesized TiO_2 NPs was examined using field-emission scanning electron microscopy (FESEM). As shown in Figure 4, all samples (C1, M1, M2, M3, and M4) exhibited relatively similar spherical particle morphologies. These observations agree with previous studies reporting that spherical TiO_2 particles are preferentially

formed under low-acidity conditions during sol–gel synthesis (Yalcin, 2022; Aida and Sreekantan, 2011).

However, a clear difference was observed between the control sample synthesized with ethanol only (C1) and the extract-assisted samples. The C1 particles tended to grow in a less controlled manner, whereas the M1–M4 samples exhibited progressively smaller and more refined particles. Quantitative particle-size analysis was performed by measuring representative particle diameters from FESEM images using ImageJ. The average particle sizes of C1, M1, M2, M3, and M4 were 152.86, 129.77, 117.17, 83.41, and 81.26 nm, respectively. This suggests that plant-derived capping agents effectively restrict particle growth during synthesis.

Figure 4 shows secondary electron images and histograms derived from ImageJ measurements. The distributions were fitted with Gaussian curves to provide insight into the particle-size distribution for each sample. C1 shows a broader distribution and a larger size range, indicating less uniform particle growth. In contrast, the extract-assisted samples, particularly M3 and M4, show a more uniform distribution and a clear shift toward smaller particle sizes. This behavior confirms that extract concentration affects particle growth and formation (Yuliarto et al., 2019).

Energy-dispersive X-ray spectroscopy (EDX) provides information on the elemental composition as provided in Figure S2 (Supplementary). The weight percentages of titanium (Ti) and oxygen (O), as presented in Table 3, are indicated by the significant peaks at the range 64-67% and 35-32%, respectively. These results suggest that the composition of the synthesized TiO_2 matches its stoichiometric formula (Sofyan et al., 2025a).

Table 3 Elemental composition of TiO_2 nanoparticles determined by EDX analysis, showing the weight percentages of titanium (Ti) and oxygen (O) for all synthesized samples

Code	Ti (wt%)	O (wt%)
C1	65.89	34.11
M1	67.05	32.95
M2	65.72	34.28
M3	65.21	34.79
M4	64.42	35.58

The extent of particle agglomeration was measured using a particle size analyzer, and the results are presented in Table 4. The particle size measurements obtained from the PSA are generally larger than those determined from FESEM images using ImageJ software. This discrepancy can be attributed to the fundamental differences between the two methods. When combined with ImageJ, FESEM provides the physical size of the nanoparticles by direct imaging, while PSA measures the hydrodynamic diameter, which encompasses the core particle plus any bound solvent molecules, capping agents, and possible agglomerates in suspension. Moreover, PSA assumes spherical, monodisperse particles, which is often not the case in real samples, leading to size distributions skewed toward larger values. Despite this difference, both FESEM and PSA results consistently demonstrated that the presence of capping agents in samples M1–M4 effectively limited particle growth compared with that in the control sample C1. These findings confirm the role of plant-based capping agents in controlling particle size and reducing nanoparticle aggregation during green synthesis (Tasisa et al., 2024).

3.4 Crystallographic Properties

X-ray diffraction (XRD) analysis was used to determine the crystalline phase and approximate crystallite size of the synthesized TiO_2 nanoparticles. The XRD patterns of the control sample, synthesized using ethanol only (C1), and the green-synthesized samples (M1–M4) are presented in Figure 5. The diffractogram shows distinct peaks corresponding to crystal planes (101), (004), (200), (105), (211), (204), and (116), which belong to pure anatase TiO_2 (JCPDS Card No. 01-071-1167). This phase is favorable for DSSC applications because of its high surface area and electronic properties, which support dye adsorption and charge transport (Eddy

et al., 2023).

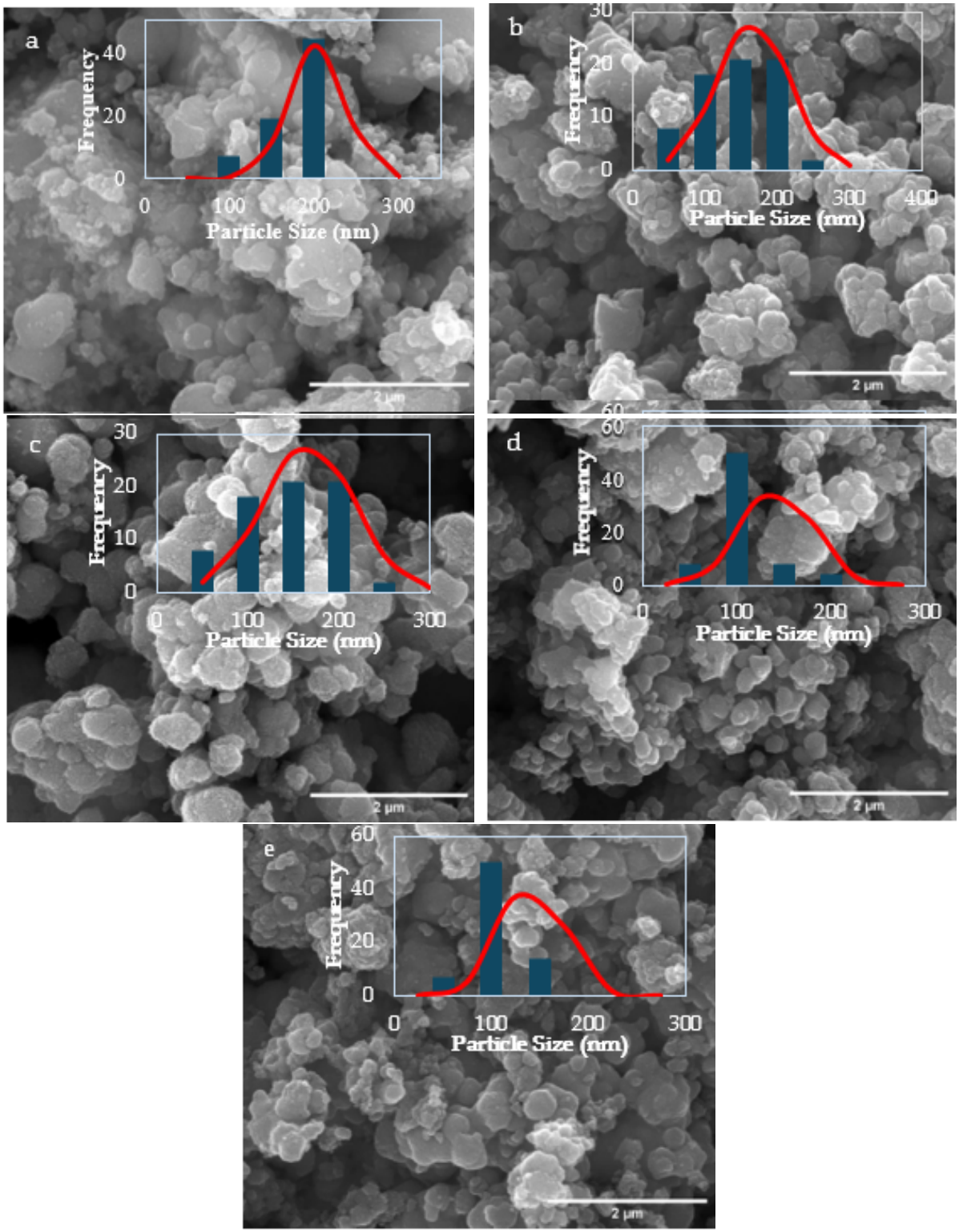

Figure 4 FESEM images of TiO_2 nanoparticles synthesized using ethanol only (a) C1 and *Melastoma malabathricum* extract with lime juice variations (b) M1, (c) M2, (d) M3, and (e) M4. The insets show particle-size distribution histograms obtained from ImageJ analysis, with a Gaussian fit (red line) illustrating the statistical distribution of particle sizes.

The mechanism underlying the exclusive formation of anatase in this study can be explained using the partial charge model. At moderately low acidity, the deprotonation of the titanium precursor species yields $[TiO(OH)(OH_2)_4]^+$, which then undergoes intramolecular deoxidation.

This promotes condensation reactions along the apical direction, resulting in a distorted octahedral chain arrangement characteristic of the anatase structure. This pathway is favored under relatively low acidity synthesis conditions, consistent with the absence of rutile peaks in the present XRD data. Therefore, the pH of the synthesis environment plays a pivotal role in directing the phase formation of TiO_2, with lower acidity facilitating anatase crystallization (El-Shear, 2017; El-Shear, 2017).

The average crystallite sizes of each nanoparticle were calculated from all diffraction peaks using the Scherrer equation (Equation 5) (Purkait et al., 2023; Zak et al., 2011) and the results are also provided in Table 4.

$$D = \frac{k\lambda}{\beta \cos\theta} \tag{5}$$

where D denotes the average crystallite size, k is Scherrer's shape constant (0.94); λ represents the wavelength of the source X-ray (0.154 nm); β corresponds to the full width at half maximum (FWHM); and θ is Bragg's diffraction angle. The average values for samples C1, M1, M2, M3, and M4 were 18.17, 14.68, 14.01, 12.56, and 12.43 nm, respectively. This decrease in crystallite size is attributed to the Melastoma malabthricum extract and lime juice that act as a capping agent, limiting the growth and agglomeration of nanoparticles (Rajendhiran et al., 2021a). These dimensions are similar to several investigations of green-synthesized TiO_2 nanoparticles (Singh et al., 2024; Singh et al., 2022; Maurya et al., 2019).

The relatively small crystallite sizes obtained in this study are considered favorable for the performance of DSSC. The combination of high surface area from the nanoscale size, nanoparticle morphology, and predominance of the anatase phase may offer more active sites for dye anchoring, which is expected to support improved charge generation in the device (Tijani et al., 2024; Eddy et al., 2023; Hegazy et al., 2016).

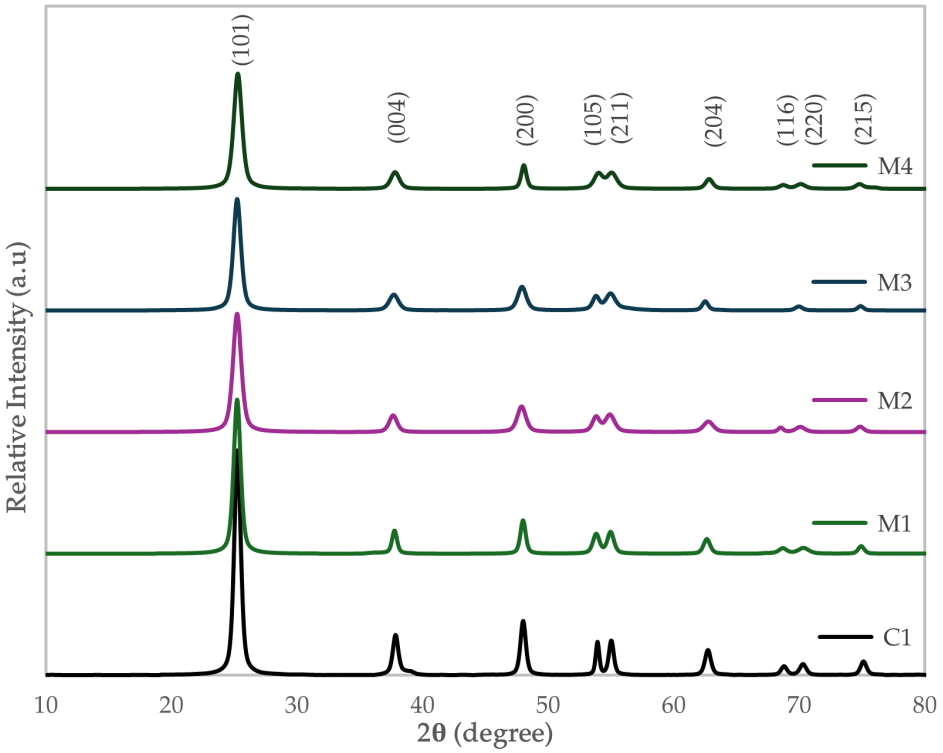

Figure 5 X-ray diffractograms of TiO_2 NPs synthesized using ethanol only (C1) and using *Melastoma malabathricum* extract with lime juice variations (M1, M2, M3, and M4)

Table 4 Average crystallite size from XRD and estimated band gap from Tauc's plot for TiO_2 nanoparticles synthesized using ethanol only (C1) and *Melastoma malabathricum* extract with lime juice variations (M1, M2, M3, and M4)

Code	Bandgap (eV)	Crystallite size (nm, XRD)	Particle Size (nm, FESEM)	Particle size (nm, PSA)
C1	3.14	18.17	152.86	409.97
M1	3.12	14.68	129.77	338.63
M2	3.09	14.01	117.17	309.33
M3	3.09	12.56	83.41	288.27
M4	3.10	12.43	81.26	340.40

3.5 Raman Spectroscopy

Raman spectroscopy was used to confirm the phase composition and chemical structure of the TiO_2 NPs. The Raman spectra of the synthesized sample were recorded in the range 800–100 cm^{-1}. The spectra of all samples in Figure 6 show prominent peaks at 144 cm^{-1}, 199 cm^{-1}, 399 cm^{-1}, 516 cm^{-1}, and 638 cm^{-1}. Thus, all of them strongly indicate the existence of the anatase phase in each sample (Su et al., 2008). The results are consistent with the X-ray diffractogram presented in Section 3.4.

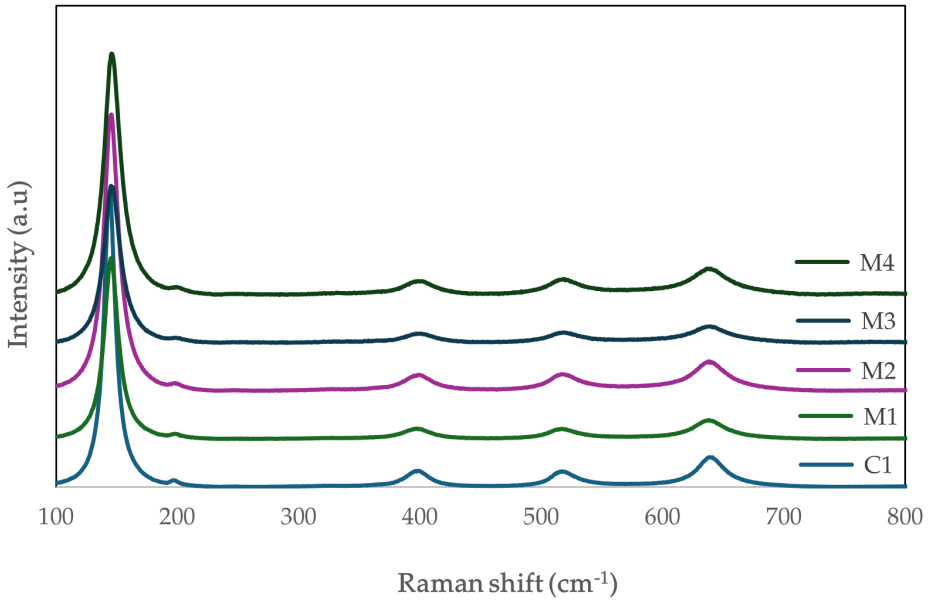

Figure 6 Raman spectra of TiO_2 NPs synthesized using ethanol only (C1) and using Melastoma malabathricum extract with lime juice variations (M1, M2, M3, and M4)

A slight blue shift is observed in the primary Raman peak, shifting from 144.2 cm^{-1} for the control sample synthesized using ethanol only (C1) to approximately 145.26 cm^{-1} for samples M1, M2, and M3, and further to 145.78 cm^{-1} for M4. This gradual shift suggests a reduction in crystallite size and potential strain effect caused by the bioactive compound (Khang and Minh, 2008; Sofyan et al., 2025b).

No D/G ratio was detected in the Raman spectra because the characteristic bands of sp^2 carbon structures around 1350 and 1580 cm^{-1} were absent. This finding is consistent with the behavior of pure anatase TiO_2 (Ruidíaz-Martínez et al., 2020). The absence of carbon is further supported by the EDS results showing only Ti and O elements in Section 3.3 and by the XRD patterns in Section 3.4. This indicates that the anatase phase is the only phase present, with no carbon-related phases. It can be concluded that the green synthesis route successfully produced high-purity anatase TiO_2 nanoparticles, with no significant incorporation

of phytochemical species into the TiO_2 lattice.

3.6 Electrochemical Properties

The electrochemical properties of the DSSC devices were evaluated using EIS to assess interfacial charge-transfer kinetics. The results are presented in the form of impedance spectra and Nyquist plots in Figure 7(a). Although the semicircles are not fully closed within the measured frequency range, clear differences in the radius of the semicircles are observed among the samples, indicating variations in the interfacial charge transfer resistance. In ascending order, the radius of the evident semicircle increases from M1 to M2, M4, M3, and C1. The corresponding estimated charge-transfer resistance (R_{ct}) is presented in Table 5 and follows the same trend. A larger Rct value indicates greater resistance to electron transfer at the interface, which may hinder charge transport and device performance (Mehmood et al., 2016). Accordingly, the lower apparent R_{ct} observed for M1 indicates a more efficient interfacial charge transfer than in the other samples.

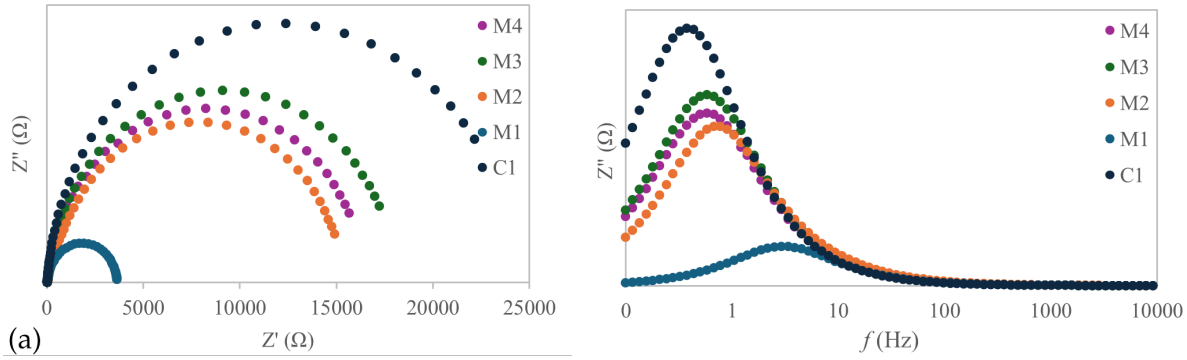

Figure 7 Nyquist (a) and Bode imaginary (b) plots of DSSC devices fabricated using TiO_2 nanoparticles synthesized using ethanol only (C1) and *Melastoma malabathricum* extract with lime juice variations (M1, M2, M3, and M4), measured under room light illumination. The Nyquist semicircle represents interfacial charge transfer at the TiO_2/dye/electrolyte interface, while the Bode peak frequency was used to estimate electron lifetime

The electron lifetime (T_e) of different TiO_2 photoanode materials was obtained using Equation (6) (Sofyan et al. 2026):

$$\tau_e = \frac{1}{2\pi f_{\max}} \tag{6}$$

where f_{max} is the phase angle's peak frequency from the Bode plot (Figure 7(b)). The extended relaxation time can be attributed to more efficient charge collection and minimum recombination losses. As described in Table 5, M2–M4 show a more balanced performance profile, with electron lifetimes ranging from 205 to 274 ms and Rct values between 14,876–17,193 Ω. This combination suggests that incorporating *Melastoma malabathricum* extract into lime juice improves charge retention while maintaining reasonable charge-transfer kinetics, consistent with the observed DSSC performance.

3.7 Photovoltaic Performance

Current density-voltage measurements as seen in Figure 8(a) reveal an intriguing correlation with the EIS results, and the corresponding photovoltaic parameters are summarized Table 6. Among all the samples, M1 exhibited the highest power conversion efficiency (PCE = 3.12%), despite its relatively low fill factor (FF = 0.38) and shorter electron lifetime (55 ms). This suggests that the M1 photoanode structure optimizes both dye loading and charge injection efficiency. In contrast, samples (M2–M4) showed more modest PCE values (2.26-2.49%), with consistently higher fill factors (FF = 0.57), which can be attributed to their longer electron

lifetimes and more balanced interfacial charge-transfer properties. The corresponding power density–voltage (P–V) curves derived from the J–V data (Figure 8(b)) further confirm these trends, with M1 delivering the highest maximum power output among the investigated photoanodes. This behavior indicates that the efficiency enhancement is primarily governed by improved photocurrent generation rather than variations in open-circuit voltage. The presence of residual organic species from the extract may partially counterbalance the beneficial effect of the chelating agent on electron transfer, which could potentially reduce effective dye adsorption or alter surface states, as reported in similar green-synthesized TiO_2 systems (Sofyan et al., 2024; Rajendhiran et al., 2021b).

Table 5 EIS parameters of DSSC devices based on TiO_2 nanoparticles synthesized using ethanol only (C1) and *Melastoma malabathricum* extract with lime juice variations (M1, M2, M3, and M4), including series resistance (R_s), estimated charge transfer resistance (R_{ct}), peak frequency (f_{max}), and electron lifetime (τ_e)

Sample	R_s (Ω)	R_{ct} (Ω)	f_{max} (Hz)	τ_e (ms)
C1	37.323	22123.836	0.374	425.809
M1	33.719	3625.759	2.910	54.722
M2	38.251	14876.175	0.778	204.639
M3	31.768	17193.234	0.580	274.331
M4	29.005	15645.045	0.580	274.331

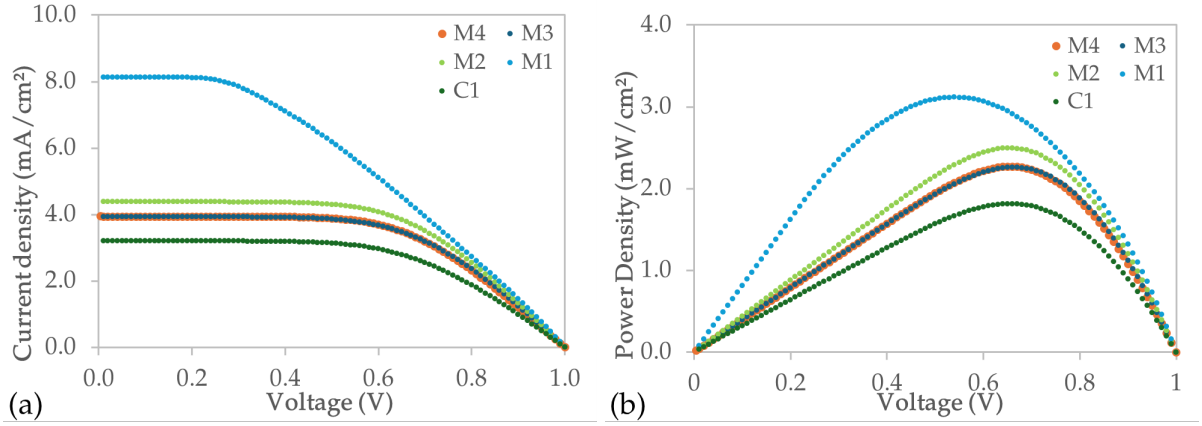

Figure 8 (a) J–V characteristics and (b) corresponding power density–voltage (P–V) curves of DSSC devices based on TiO_2 nanoparticles synthesized using ethanol only (C1) and *Melastoma malabathricum* extract with lime juice variations (M1, M2, M3, and M4), recorded under standard illumination conditions (100 mW cm^{-2}).

The future of green synthesis is closely linked to the global push for sustainable, eco-friendly technologies. This approach uses naturally derived reducing and capping agents, thereby avoiding hazardous chemicals and making the process safer for human health and the environment. Although dye-sensitized solar cells (DSSCs) are currently less efficient than other photovoltaic technologies, they remain valuable for applications where efficiency is not the main priority. Examples include indoor energy harvesting under low-light conditions to power small electronic devices; wearable electronics, where their lightweight and flexible design enables integration into smart textiles; building-integrated photovoltaics, such as transparent solar panels for windows and facades that combine functionality with aesthetics; and low-power sensors for remote monitoring, where energy requirements are minimal.

To evaluate the performance of the DSSCs developed in this study relative to similar systems, their photovoltaic characteristics are compared with those of previously reported devices that employed green-synthesized TiO_2 photoanodes. Table 7 presents the results of this benchmarking. By placing the current findings alongside earlier reports, the comparison shows how key

material properties—such as crystallite size and interfacial charge-transfer resistance—directly influence overall device efficiency. The table highlights how different plant-derived synthesis routes affect these parameters, revealing the link between the microstructural features of TiO_2 photoanodes and PV performance.

Table 6 Photovoltaic parameters of DSSC devices based on TiO_2 nanoparticles synthesized using ethanol only (C1) and *Melastoma malabathricum* extract with lime juice variations (M1, M2, M3, and M4) under standard illumination (100 mW cm^{-2})

Sample	I_{sc} (mA)	V_{oc} (V)	I_{max} (mA)	V_{max} (V)	J_{sc} (mA/cm^2)	FF	PCE (%)	I_{sc} (mA)
C1	3.20	1.00	2.75	0.66	3.2	0.57	1.81	3.20
M1	8.13	1.00	5.77	0.54	8.13	0.38	3.12	8.13
M2	4.38	1.00	3.84	0.65	4.38	0.57	2.49	4.38
M3	3.93	1.00	3.42	0.66	3.93	0.57	2.26	3.93
M4	3.95	1.00	3.43	0.66	3.95	0.57	2.27	3.95

Table 7 Comparative benchmark of green-synthesized TiO_2 photoanodes derived from different plant parts, summarizing TiO_2 phase, crystallite size, charge-transfer resistance (Rct), and power conversion efficiency (PCE) reported in this study and other similar studies

Plant Species	Plant Part	Variation	TiO_2 Phase	Crystallite Size (nm)	Rct (Ω)	PCE (%)	Ref
Melastoma malabathricum	Fruit	Extract	Anatase	14.68	3625.78	3.12	This Study
		Extract + 20% lime juice	Anatase	14.01	14876.17	2.49	
		Extract + 40% lime juice	Anatase	12.56	17193.23	2.26	
		Extract + 50% lime juice	Anatase	12.43	15645.05	2.27	
Saccharum officinarum	Sugarcane	Water	Anatase	8.76	16.87	0.68	(Singh et al., 2024)
		Water + sugarcane juice	Anatase	5.99	7.21	1.29	
		Sugarcane juice	Anatase	7.65	6.68	3.65	
Citrus limon	Fruit	0.9% juice extract	Anatase	10.00	43.35	3.87	(Singh et al., 2022)
		0.45% juice extract	Anatase	8.00	50.23	4.55	
		0.27% juice extract	Anatase	11.00	31.34	2.73	
Gambir leaves	Leaf	Extract	Anatase	9.23	66.77	4.10	(Sofyan et al., 2025b)
		Extract + 10% Acetylacetone	Anatase	8.24	42.83	2.42	
		Extract + 30% Acetylacetone	Anatase	8.37	92.84	2.09	
		Extract + 50% Acetylacetone	Anatase	7.19	92.84	4.40	

4. Conclusions

This study demonstrates that bio-derived chelating agents can systematically tune the properties of TiO_2 photoanodes, offering a scalable strategy for sustainable DSSC fabrication. Melas-

toma malabathricum fruit extract, as a reducing and capping agent, and lime juice, as a chelating agent, were shown to produce anatase-phase TiO_2 NPs. Variations of extract composition were found to inhibit crystallite and particle growth of TiO_2 NPs, though aggregation still occurred to some extent. The DSSC devices showed a clear improvement in photovoltaic performance compared with the control sample, achieving an efficiency of 3.12% for the TiO_2 photoanode synthesized without lime juice. While samples synthesized with lime juice exhibited better charge retention, their efficiencies were slightly lower (2.26–2.49%), highlighting a trade-off between charge transport and light harvesting. These findings provide valuable guidance for future DSSC development, particularly in the design of bio-capped TiO_2 photoanodes. Future research could explore the optimal performance achievable by combining the exceptional light-harvesting capability observed in samples without lime juice with the enhanced charge-preservation properties demonstrated by samples synthesized with lime-juice extract. This work demonstrates the promise of green synthesis routes for developing efficient, environmentally friendly photovoltaic materials while providing clear strategies for further performance enhancement.

Acknowledgements

One of the authors, Muhammad, acknowledges the Indonesia Endowment Fund for Education (LPDP) for funding his study and publication under Doctoral Scholarship No. 0016464/TRP/D/19/lpdp2023.

Author Contributions

Muhammad: Writing – original draft, Investigation, Data curation, Nofrijon Sofyan: Writing – review & editing, Validation, Methodology, Formal analysis, Conceptualization, Mouna M'Rad: Data curation, Akhmad Herman Yuwono: Writing – review & editing. Donanta Dhaneswara: Writing – review & editing.

Conflict of Interest

The authors declare that they have no known competing financial interests or personal relationships that could have appeared to influence the work reported in this paper.

References

Aida, I. S., & Sreekantan, S. (2011). Effect of pH on TiO_2 nanoparticles via sol gel method. *Advanced Materials Research*, *173*(173), 184–189.

Bellè, U., Spini, D., Del Curto, B., Pedeferri, M. P., & Diamanti, M. V. (2023). Water-Based Photocatalytic Sol–Gel TiO_2 Coatings: Synthesis and Durability. *Catalysts*, *13*(3). https://doi.org/10.3390/catal13030494

Bhagoria, P., Sebastian, E. M., Jain, S. K., Purohit, J., & Purohit, R. (2019). Nanolithography and its alternate techniques. In *Materials today: Proceedings* (pp. 3048–3053). Elsevier Ltd. https://doi.org/10.1016/j.matpr.2020.02.633

Boediman, A., Rahadi, R. A., & Nugraha, B. A. (2021). An Overview of Indonesian Renewable Energy Studies and Its Investment Opportunities. *Indonesian Journal of Energy*, *4*(2), 87–100.

Devadiga, D., Selvakumar, M., Shetty, P., & Santosh, M. S. (2021). Dye-Sensitized Solar Cell for Indoor Applications: A Mini-Review. *Journal of Electronic Materials*, *50*(6), 3187–3206. https://doi.org/10.1007/s11664-021-08854-3

Drygala, A. (2021). Influence of TiO_2 film thickness on photovoltaic properties of dye-sensitized solar cells. In *Iop conference series: Earth and environmental science*. IOP Publishing Ltd. https://doi.org/10.1088/1755-1315/642/1/012001

Dülger, B., Özkan, G., Angı, O. S., & Özkan, G. (2024). Green synthesis of TiO_2 nanoparticles using Aloe Vera extract as catalyst support material and studies of their catalytic activity

in dehydrogenation of Ethylenediamine Bisborane. *International Journal of Hydrogen Energy*. https://doi.org/10.1016/j.ijhydene.2024.02.223

Eddy, D. R., Permana, M. D., Sakti, L. K., Sheha, G. A. N., Solihudin, G. A. N., Hidayat, S., Takei, T., Kumada, N., & Rahayu, I. (2023). Heterophase Polymorph of TiO_2 (Anatase, Rutile, Brookite, TiO_2 (B)) for Efficient Photocatalyst: Fabrication and Activity. *Nanomaterials*, *13*(4). https://doi.org/10.3390/nano13040704

El-Shear, A.-H. (2017). Influence of pH on the Formulation of TiO_2 Nanocrystalline Powders. *American Journal of Materials Synthesis and Processing*, *2*(4), 51. https://doi.org/10.11648/j.ajmsp.20170204.11

Hegazy, A., Kinadjian, N., Sadeghimakki, B., Sivoththaman, S., Allam, N. K., & Prouzet, E. (2016). TiO_2 nanoparticles optimized for photoanodes tested in large area Dye-sensitized solar cells (DSSC). *Solar Energy Materials and Solar Cells*, *153*, 108–116. https://doi.org/10.1016/j.solmat.2016.04.004

Hendinata, L. K., Prilia, R., Fikri, A. I. R., Suprapto, M. A., & Siddiq, N. A. (2024). Evaluating the Energy Performance of Transparent Photovoltaics for Building Windows in Tropical Climates. *Indonesian Journal of Energy*, *7*(2). https://doi.org/10.33116/ije.v7i2.192

Hussain, S. A., Razi, F., Hewage, K., & Sadiq, R. (2023). The perspective of energy poverty and 1st energy crisis of green transition. *Energy*, *275*. https://doi.org/10.1016/j.energy.2023.127487

Ibrahim, M. H., Salim, M. R., Mohd Nor, M. Y., Abdullah, A. S., & Azmi, A. I. (2025). Quaternary chalcogenides as transport layers in solid-state DSSC: a feasibility study. *Chalcogenide Letters*, *22*(6), 551–560. https://doi.org/10.15251/CL.2025.226.551

Isnaini, I., Yasmina, A., & Nur'amin, H. W. (2019). Antioxidant and cytotoxicity activities of karamunting (Melastoma malabathricum L.) fruit ethanolic extract and quercetin. *Asian Pacific Journal of Cancer Prevention*, *20*(2), 639–643. https://doi.org/10.31557/APJCP.2019.20.2.639

Karim, N. A., Mehmood, U., Zahid, H. F., & Asif, T. (2019). Nanostructured photoanode and counter electrode materials for efficient Dye-Sensitized Solar Cells (DSSCs). *Solar Energy*, *185*, 165–188. https://doi.org/10.1016/j.solener.2019.04.057

Kaur, H., Kaur, S., Singh, J., Rawat, M., & Kumar, S. (2019). Expanding horizon: Green synthesis of TiO_2 nanoparticles using Carica papaya leaves for photocatalysis application. *Materials Research Express*, *6*(9). https://doi.org/10.1088/2053-1591/ab2ec5

Khang, N. C., & Minh, N. V. (2008). Synthesis of Anatase TiO_2 Particles and Their Size-Related Structural, Optical, and Raman Spectroscopy Studies. *Journal of Nonlinear Optical Physics & Materials*, *17*(2), 167–174.

Liu, Y. S., Chang, Y. C., & Chen, H. H. (2018). Silver nanoparticle biosynthesis by using phenolic acids in rice husk extract as reducing agents and dispersants. *Journal of Food and Drug Analysis*, *26*(2), 649–656. https://doi.org/10.1016/j.jfda.2017.07.005

Makuła, P., Pacia, M., & Macyk, W. (2018). How To Correctly Determine the Band Gap Energy of Modified Semiconductor Photocatalysts Based on UV-Vis Spectra. *Journal of Physical Chemistry Letters*, *9*(23), 6814–6817. https://doi.org/10.1021/acs.jpclett.8b02892

Marslin, G., Siram, K., Maqbool, Q., Selvakesavan, R. K., Kruszka, D., Kachlicki, P., & Franklin, G. (2018). Secondary metabolites in the green synthesis of metallic nanoparticles. *Materials*, *11*(6). https://doi.org/10.3390/ma11060940

Maurya, I. C., Singh, S., Senapati, S., Srivastava, P., & Bahadur, L. (2019). Green synthesis of TiO_2 nanoparticles using Bixa orellana seed extract and its application for solar cells. *Solar Energy*, *194*, 952–958. https://doi.org/10.1016/j.solener.2019.10.090

Mehmood, U., Aslam, H. Z., Al-Sulaiman, F. A., Al-Ahmed, A., Ahmed, S., Malik, M. I., & Younas, M. (2016). Electrochemical Impedance Spectroscopy and Photovoltaic Analyses of Dye-Sensitized Solar Cells Based on Carbon/TiO_2 Composite Counter Electrode. *Journal of The Electrochemical Society*, *163*(5), H339–H342. https://doi.org/10.1149/2.0111606jes

Muhammad, Sofyan, N., Yuwono, A. H., & Dhaneswara, D. (2025). A review on green synthesis of TiO_2 nanoparticles: enhancing DSSC performance and exploring future opportunities. *Materials Science for Energy Technologies*, *8*, 188–199. https://doi.org/10.1016/j.mset.2025.07.001

Nagaraj, G., Raj, A. D., Albert, I., & Josephine, R. L. (2019). Tuning the optical band Gap of pure TiO_2 via photon induced method. *Optik*, *179*, 889–894. https://doi.org/10.1016/j.ijleo.2018.11.009

Na-Phattalung, S., Harding, D. J., Pattanasattayavong, P., Kim, H., Lee, J., Hwang, D. W., Chung, T. D., & Yu, J. (2022). Band gap narrowing of TiO_2 nanoparticles: A passivated Co-doping approach for enhanced photocatalytic activity. *Journal of Physics and Chemistry of Solids*, *162*. https://doi.org/10.1016/j.jpcs.2021.110503

Polte, J. (2015). Fundamental growth principles of colloidal metal nanoparticles - a new perspective. *CrystEngComm*, *17*(36), 6809–6830. https://doi.org/10.1039/c5ce01014d

Purkait, P. K., Majumder, S., Roy, S., Maitra, S., Chandra Das, G., & Chaudhuri, M. G. (2023). Enhanced heterogeneous photocatalytic degradation of florasulam in aqueous media using green synthesized TiO_2 nanoparticle under UV light irradiation. *Inorganic Chemistry Communications*, *155*. https://doi.org/10.1016/j.inoche.2023.111017

Rababah, H. E., Ghazali, A., & Isa, M. H. M. (2021). Building integrated photovoltaic (BIPV) in southeast asian countries: Review of effects and challenges. *Sustainability (Switzerland)*, *13*(23). https://doi.org/10.3390/su132312952

Rajendhiran, R., Deivasigamani, V., Palanisamy, J., Masan, S., & Pitchaiya, S. (2021a). Terminalia catappa and carissa carandas assisted synthesis of TiO_2 nanoparticles - A green synthesis approach. In *Materials today: Proceedings* (pp. 2232–2238). Elsevier Ltd. https://doi.org/10.1016/j.matpr.2020.10.223

Rajendhiran, R., Deivasigamani, V., Palanisamy, J., Pitchaiya, S., Eswaramoorthy, N., & Masan, S. (2021b). Plectranthus amboinicus Leaf Extract Synthesized Spherical like-TiO_2 Photoanode for Dye-Sensitized Solar Cell Application. *Silicon*, *13*(10), 3329–3336. https://doi.org/10.1007/s12633-020-00709-6

Rao, G. K., Ashok, C., Rao, K. V., Chakra, C. S., & Tambur, P. (2015). Green Synthesis of TiO_2 Nanoparticles Using Aloe Vera Extract. *International Journal of Advanced Research in Physical Science*, *2*, 28–34.

Roy, A., Mukhopadhyay, S., Devi, P. S., & Sundaram, S. (2019). Polyaniline-Layered Rutile TiO_2 Nanorods as Alternative Photoanode in Dye-Sensitized Solar Cells. *ACS Omega*, *4*(1), 1130–1138. https://doi.org/10.1021/acsomega.8b02628

Ruidíaz-Martínez, M., Álvarez, M. A., López-Ramón, M. V., Cruz-Quesada, G., Rivera-Utrilla, J., & Sánchez-Polo, M. (2020). Hydrothermal synthesis of RGO-TiO_2 composites as high-performance UV photocatalysts for ethylparaben degradation. *Catalysts*, *10*(5). https://doi.org/10.3390/catal10050520

Saini, R., & Kumar, P. (2023). Green synthesis of TiO_2 nanoparticles using Tinospora cordifolia plant extract & its potential application for photocatalysis and antibacterial activity. *Inorganic Chemistry Communications*, *156*. https://doi.org/10.1016/j.inoche.2023.111221

Sangeetha, A., Ambli, A., & Nagabhushana, B. M. (2024). Green and chemical synthesis of TiO_2 nanoparticles: An In-depth comparative analysis and photoluminescence study. *Nano-Structures and Nano-Objects*, *40*. https://doi.org/10.1016/j.nanoso.2024.101408

Septiningrum, F., Fahirah, R., Yuwono, A. H., Muhammad, M., Sofyan, N., Dhaneswara, D., Jap, N., & Priambodo, D. P. (2026). Unravelling How pH Sequence Shapes Green-Synthesized TiO_2 Nanoparticles for Dye-Sensitized Solar Cells. *International Journal of Technology*, *17*(1), 145. https://doi.org/10.14716/ijtech.v17i1.8206

Siagian, P., Alam, H., Fahreza, M., & Tampubolon, R. J. (2024). Peningkatan Daya Panel Surya Dengan Konsentrator Cahaya dari Bahan Aluminium Foil. *Jurnal Serambi Engineering*, *9*(2), 8490–8498.

Singh, P., Sharma, S., & Srivastava, P. (2024). Natural Saccharum officinarum (sugarcane) juice assisted TiO_2 nanoparticle synthesis for high performance dye-sensitized solar cell. *Optical Materials*, *147*. https://doi.org/10.1016/j.optmat.2023.114685

Singh, S., Maurya, I. C., Tiwari, A., Srivastava, P., & Bahadur, L. (2022). Green synthesis of TiO_2 nanoparticles using Citrus limon juice extract as a bio-capping agent for enhanced performance of dye-sensitized solar cells. *Surfaces and Interfaces*, *28*. https://doi.org/10.1016/j.surfin.2021.101652

Sofyan, N., Jamil, A. M., Ridhova, A., Yuwono, A. H., Dhaneswara, D., & Fergus, J. W. (2024). Graphene oxide doping in tropical almond (Terminalia catappa L.) fruits extract mediated green synthesis of TiO_2 nanoparticles for improved DSSC power conversion efficiency. *Heliyon*, *10*(8). https://doi.org/10.1016/j.heliyon.2024.e29370

Sofyan, N., Muhammad, Ridhova, A., Angellinnov, F., M'rad, M., Yuwono, A. H., Dhaneswara, D., Priyono, B., & Fergus, J. W. (2025a). Jasmine flowers extract mediated green synthesis of TiO_2 nanoparticles and their photocurrent characteristics for dye-sensitized solar cell application. *Materials for Renewable and Sustainable Energy*, *14*(2). https://doi.org/10.1007/s40243-025-00320-y

Sofyan, N., Ridhova, A., Yuwono, A. H., & Udhiarto, A. (2017). Fabrication of Solar Cells With TiO_2 Nanoparticles Sensiztized Using Natural Dye Extracted From Mangosteen Pericarps. *International Journal of Technology*, *8*(7), 1229–1238.

Sofyan, N., Rilda, Y., Andriayani, Angellinnov, F., M'rad, M., Muhammad, Ridhova, A., Herman Yuwono, A., & Dhaneswara, D. (2025b). Sustainable Synthesis of TiO_2 Nanoparticles from Gambier Leaf Extract for Enhanced DSSC Photocurrent Response. *Results in Materials*, 100752. https://doi.org/10.1016/j.rinma.2025.100752

Su, W., Zhang, J., Feng, Z., Chen, T., Ying, P., & Li, C. (2008). Surface phases of TiO_2 nanoparticles studied by UV raman spectroscopy and FT-IR spectroscopy. *Journal of Physical Chemistry C*, *112*(20), 7710–7716. https://doi.org/10.1021/jp7118422

Szindler, M., Szindler, M., Drygała, A., Lukaszkowicz, K., Kaim, P., & Pietruszka, R. (2021). Dye-sensitized solar cell for building-integrated photovoltaic (BIPV) applications. *Materials*, *14*(13). https://doi.org/10.3390/ma14133743

Tasisa, Y. E., Sarma, T. K., Krishnaraj, R., & Sarma, S. (2024). Band gap engineering of titanium dioxide (TiO_2) nanoparticles prepared via green route and its visible light driven for environmental remediation. *Results in Chemistry*, *11*. https://doi.org/10.1016/j.rechem.2024.101850

Thiurunavukkarau, R., Shanmugam, S., Subramanian, K., Pandi, P., Muralitharan, G., Arokiarajan, M., Kasinathan, K., Sivaraj, A., Kalyanasundaram, R., AlOmar, S. Y., & Shanmugam, V. (2022). Silver nanoparticles synthesized from the seaweed Sargassum polycystum and screening for their biological potential. *Scientific Reports*, *12*(1). https://doi.org/10.1038/s41598-022-18379-2

Tijani, N. A., Hokello, J., Awojobi, K. O., Marnadu, R., Shkir, M., Ahmad, Z., Afolabi, A. O., Adewinbi, S. A., & Adebayo, I. A. (2024). Recent advances in Mushroom-mediated nanoparticles: A critical review of mushroom biology, nanoparticles synthesis, types, characteristics and applications. *Journal of Drug Delivery Science and Technology*, *96*. https://doi.org/10.1016/j.jddst.2024.105695

Tyas, L. K., Suryana, R., Nurosyid, F., & Ilahi, N. A. (2017). Comparison of Titanium Dioxide (TiO_2) nanoparticle-nanofiber and nanofiber-nanoparticle on the application of dye-sensitized solar cell (DSSC). In *Journal of physics: Conference series*. Institute of Physics Publishing. https://doi.org/10.1088/1742-6596/795/1/012019

Villanueva-Cab, J., Olalde-Velasco, P., Romero-Contreras, A., Zhuo, Z., Pan, F., Rodil, S. E., Yang, W., & Pal, U. (2018). Photocharging and Band Gap Narrowing Effects on the Performance of Plasmonic Photoelectrodes in Dye-Sensitized Solar Cells. *ACS Applied Materials and Interfaces*, *10*(37), 31374–31383. https://doi.org/10.1021/acsami.8b10063

Xu, K., & Chen, J. (2020). High-resolution scanning probe lithography technology: a review. *Applied Nanoscience (Switzerland)*, *10*(4), 1013–1022. https://doi.org/10.1007/s13204-019-01229-5

Yadav, B. C., Singh, S., & Yadav, T. P. (2015). Titania prepared by ball milling: Its characterization and application as liquefied petroleum gas sensor. *Synthesis and Reactivity in Inorganic, Metal-Organic and Nano-Metal Chemistry*, *45*(4), 487–494. https://doi.org/10.1080/15533174.2012.749892

Yalcin, M. (2022). The effect of pH on the physical and structural properties of TiO_2 nanoparticles. *Journal of Crystal Growth*, *585*. https://doi.org/10.1016/j.jcrysgro.2022.126603

Yan, X., Feng, L., Jia, J., Zhou, X., & Lin, Y. (2013). Controllable synthesis of anatase TiO_2 crystals for high-performance dye-sensitized solar cells. *Journal of Materials Chemistry A*, *1*(17), 5347–5352. https://doi.org/10.1039/c3ta01621h

Yuliarto, B., Septiani, N. L. W., Kaneti, Y. V., Iqbal, M., Gumilar, G., Kim, M., Na, J., Wu, K. C. W., & Yamauchi, Y. (2019). Green synthesis of metal oxide nanostructures using naturally occurring compounds for energy, environmental, and bio-related applications. *New Journal of Chemistry*, *43*(40), 15846–15856. https://doi.org/10.1039/c9nj03311d

Yum, J. H., Baranoff, E., Wenger, S., Nazeeruddin, M. K., & Grätzel, M. (2011). Panchromatic engineering for dye-sensitized solar cells. *Energy and Environmental Science*, *4*(3), 842–857. https://doi.org/10.1039/c0ee00536c

Zak, A. K., Majid, W. H. A., Abrishami, M. E., & Yousefi, R. (2011). X-ray analysis of ZnO nanoparticles by Williamson-Hall and size-strain plot methods. *Solid State Sciences*, *13*(1), 251–256. https://doi.org/10.1016/j.solidstatesciences.2010.11.024

Zanatta, A. R. (2019). Revisiting the optical bandgap of semiconductors and the proposal of a unified methodology to its determination. *Scientific Reports*, *9*(1), 11225. https://doi.org/10.1038/s41598-019-47670-y